The magnetoelectrochemical switch

Petru Lunca Popa[a,1], Neil T. Kemp[b,1], Hicham Majjad[c], Guillaume Dalmas[c], Vina Faramarzi[c], Christian Andreas[c,d], Riccardo Hertel[c], and Bernard Doudin[c,2]

[a]Département Science et Analyse des Matériaux, Centre de Recherche Public Gabriel Lippmann, L-4422 Belvaux, Luxembourg; [b]Department of Physics, University of Hull, Kingston-upon-Hull HU6 7RX, United Kingdom; [c]Institut de Physique et Chimie des Matériaux de Strasbourg (IPCMS) and Laboratory of Nanostructures in Interaction with their Environment (NIE), University of Strasbourg, UMR 7504 CNRS-UdS, 67034 Strasbourg, France; and [d]Peter Grünberg Institut, Forschungszentrum Jülich GmbH, 52428 Jülich, Germany

Edited* by J. M. D. Coey, Trinity College Dublin, Dublin, Ireland, and approved June 20, 2014 (received for review December 12, 2013)

In the field of spintronics, the archetype solid-state two-terminal device is the spin valve, where the resistance is controlled by the magnetization configuration. We show here how this concept of spin-dependent switch can be extended to magnetic electrodes in solution, by magnetic control of their chemical environment. Appropriate nanoscale design allows a huge enhancement of the magnetic force field experienced by paramagnetic molecular species in solutions, which changes between repulsive and attractive on changing the electrodes' magnetic orientations. Specifically, the field gradient force created within a sub-100-nm-sized nanogap separating two magnetic electrodes can be reversed by changing the orientation of the electrodes' magnetization relative to the current flowing between the electrodes. This can result in a breaking or making of an electric nanocontact, with a change of resistance by a factor of up to 10^3. The results reveal how an external field can impact chemical equilibrium in the vicinity of nanoscale magnetic circuits.

magnetohydrodynamics | supramolecular chemistry | electrochemistry

Spintronics (1, 2) is a mature research field in solid-state physics, with important electronic device applications. Spin-dependent transport studies in a liquid environment are much scarcer, and still rely on solid-state spintronics devices concepts. For example, giant magnetoresistance or tunnel magnetoresistance spin valves (3) are used for detecting the stray magnetic field (4) of nearby micrometer-sized (bioactive) magnetic beads (5). The objects studied are significantly larger than the molecular scale, owing to the predominant concentration gradient and Brownian forces exceeding by orders of magnitudes the magnetic force experienced by paramagnetic molecules (6). However, miniaturization of ferromagnetic elements below the micrometer range provides opportunities for enhancing the magnetic force field, making the detection of single spin possible (7). We propose here to use such a nanoscale enhancement strategy to investigate how the realization of very large magnetic field gradients can impact the properties of paramagnetic molecules, in particular by modifying their chemical equilibrium. An external magnetic field controls the magnetization direction of ferromagnetic immersed electrodes, with a related large change of the magnetic forces in their vicinity. This modifies accordingly the chemical stability of the solution, in the interesting case where paramagnetic molecules are essential to the construction of a conductive molecular-sized system. The resulting metallic nanobridge therefore exhibits electrical properties tunable through a change of magnetic orientations of the electrodes. While it relies on a totally different physical origin, this is the chemical analog of a solid-state spin valve device.

We illustrate this concept by presenting magnetoresistance (MR) results for a Ni-based nanobrige separating two nearby Ni electrodes immersed in an electrochemical solution. The experiments are based upon reduction (oxidation) of Ni^{++} ions (Ni metal) on these electrodes used as working electrodes kept under potentiostatic conditions in an electrochemical cell, with MR investigations performed after an electrodeposited metallic Ni bridge is stabilized between the two nearby electrodes. Lab-on-chip microfluidic circuitry directs the electrolyte flow (Fig. 1), with an external valve system allowing change of the chemical environment. Since measurements are performed in situ in an electrolyte, we take advantage of microfluidic control of the composition of the bath to reveal unambiguously how a change in the chemical bath impacts the MR properties.

The two facing planar electrodes are first patterned with a typical separation in the 50- to 100-nm range. They serve as working electrodes (W_1 and W_2, Fig. 1) and share the same imposed potentiostatic conditions for reducing metal ions in solutions. Electrodeposition of a metallic film of thickness in the range of the separation between electrodes results in the fabrication of a metallic nanobridge (Fig. 1). Full data and details for fabricating Ni, Co, or Ag metallic nanobridges down the few atoms size are presented in our previous work (8–11), and more details are given in *SI Text*. More specifically, diminution of the initial gap between the two nearby patterned working electrodes occurs by reduction of Ni^{++} ions under constant negative potential V_{close}, referred to a Pt or Ag/Cl electrode (R, Fig. 1). It results in electroplating a Ni film of 20- to 50-nm thickness over the whole surface of the two electrodes W_1 and W_2. A small superimposed monitoring ac excitation between W_1 and W_2 provides a diagnostic of the impedance separating W_1 and W_2 and reveals the making or breaking of the Ni bridge. A clear transition from a capacitive behavior to a purely resistive contact occurs below several kiloohms impedance value. The ac conductance plotted in Fig. 1 corresponds to the real part of the impedance diagnostic measurement and is not indicative of the dc electrolytic current in the cell. If a less negative voltage is

Significance

The magnetic gradient force field offers numerous possibilities to position and manipulate magnetic nanoparticles, but has limited influence on paramagnetic molecules in solutions. We argue here that proper design and miniaturization of ferromagnetic electrodes create huge force fields in their vicinity, tunable by an external magnetic field. We illustrate this concept by presenting how the conduction of a Ni metallic nanobridge is drastically modified by the Ni redox reactions equilibrium shifted under magnetic control, creating the chemical equivalent of the solid-state spin valve device. While the importance of the magnetic field amplitude on chemical reactions is well documented, our findings suggest that the magnetic field gradient can become a dominant influencing factor on chemical reactions at the nanoscale.

Author contributions: P.L.P., N.T.K., H.M., G.D., V.F., C.A., R.H. and B.D. performed research, analyzed data and wrote the paper.

The authors declare no conflict of interest.

*This Direct Submission article had a prearranged editor.

[1]P.L.P. and N.T.K. contributed equally to this work.

[2]To whom correspondence should be addressed. Email: bdoudin@unistra.fr.

This article contains supporting information online at www.pnas.org/lookup/suppl/doi:10.1073/pnas.1322828111/-/DCSupplemental.

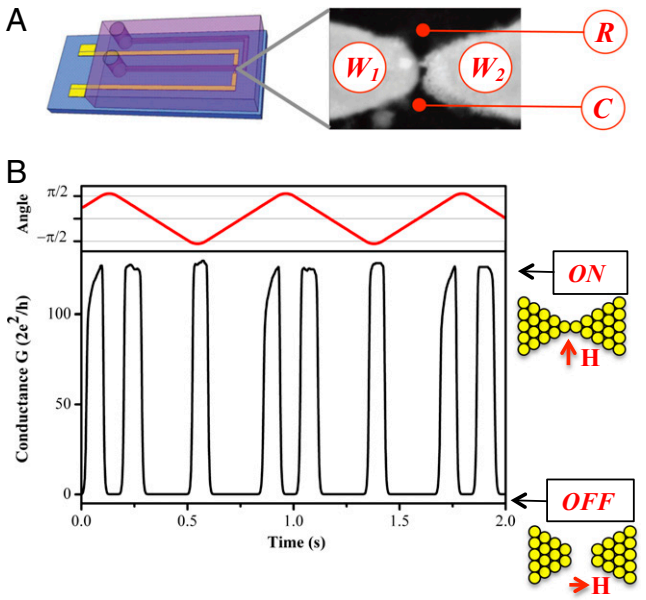

Fig. 1. Ni nanocontact construction, with *ON*/*OFF* switching of its conductance when varying the direction of the external magnetic field. (*A*) Sketch of the microfluidic cell, with electron microscopy zoom of the nanoelectrodes used as working electrodes W_1, W_2 in an electrochemical cell including a reference *R* and a counter *C* electrode. (*B*) Time evolution of the conductance under oscillating (0.5 Hz) rotation of the applied magnetic field of constant 0.8-T amplitude. The top line represents the time oscillation of the magnetic field orientation, with an opening of the contact when the field is along the direction of the electrodes (zero angle) and closure at angles in the vicinity of $\pm\pi/2$. The diagrams on the right present schematics of the related open (*OFF*) and closed (*ON*) nanocontacts.

applied, the contact can reopen when oxidation of the metallic Ni bridge prevails, at V_{open}. Control and stabilization of the contact impedance is obtained by an iterative step approximation. The typical procedure is to close a contact, and then reach a potentiostatic condition to a value V_{stable}, using 10-mV step increments, until the conductance of the nanometer-size Ni bridge remains stable over a typical 10^3-s time scale, with the sample impedance in the range 10–1000 Ω. The MR properties are then measured under external magnetic field sweep or magnetic field rotation, furthermore monitored while exchanging the high concentration Ni electrolyte with a solution containing the boric acid buffer only, keeping the bath pH around 4. Data are shown in conductance values in units of the quantum of conductance $G_0 = 2e^2/h \sim 1/13$ kΩ, following the literature of quantum ballistic transport studies in metallic nanocontacts (12).

Changing the direction of the saturating applied magnetic field has a dramatic influence on the conductance of Ni nanocontacts (Fig. 1). For sufficiently large field values (0.8 T in our case), the electrodes are magnetized in a well-defined saturated state along the applied field. Changing the field direction results in switching between the *OFF* conduction state of the sample when the field is longitudinal to the current direction (zero angle), and the *ON* state when transverse. The *ON*/*OFF* conductance ratio reaches 10^3, limited by the *OFF* leakage current resulting from the finite impedance between working and reference electrodes (measured in a typical 10^5-Ω range by impedance spectroscopy at frequencies below 1 kHz).

Fig. 2 details how this large anisotropic magnetoresistance (AMR) relies on the presence of Ni ions in solution. Microfluidic control allows a reversible change of the Ni ions concentration, keeping the monitoring of the AMR properties. Region I of Fig. 2 corresponds to the data shown in Fig. 1*B*, with a reconstruction of the AMR curve from the time-dependent angle of the applied field synchronized with the time-dependent sample conductance values (Fig. 2*B*). The large oscillations disappear when the closed *ON* state is realized with the buffer electrolyte only present in the solution (Fig. 2, region II). For bulk metallic Ni, the AMR does not exceed a few percent, and follows a simple $\cos^2$ shape, signature of the influence of spin-orbit interactions on diffusive electric transport (13). This is indeed observed in the AMR reconstruction curve of region II (Fig. 2*C*), confirming that the sample is made of a metallic Ni contact, and that magnetostriction artifacts do not affect the observed properties (14). A remarkable recovery of the large AMR properties is found when reinserting the Ni ions in the solution (Fig. 2, region III).

Another set of experiments was performed under variable magnitude magnetic field, which is the typical magnetoresistance measurement method for spin valve devices (Fig. 3): The MR curves in regions 1 and 2 of Fig. 3*A* reflect the AMR properties under the assumption that the low-field magnetic configuration does not correspond any more to the well-aligned saturation state. For the case of Fig. 3, a low conductance is expected in the longitudinal magnetization state pinned at high fields. Partial magnetization rotation occurs at lower fields, with the transverse orientation increasing significantly the conductance, as previously indicated in the data of Fig. 2 (15). The data of Fig. 3 *B* and *C* also confirm the impressive long-term device stability: The memory of the MR properties of the first stage of the experiment (region 1 of Fig. 3*A*) is nearly perfectly recovered in region 2 even though the contact spent 600 s opened (*OFF* state) when Ni ions were eliminated from the bath. A closer inspection of the evolution of the AMR after exchanging the solution reveals that the disappearance (reappearance) of the large AMR is

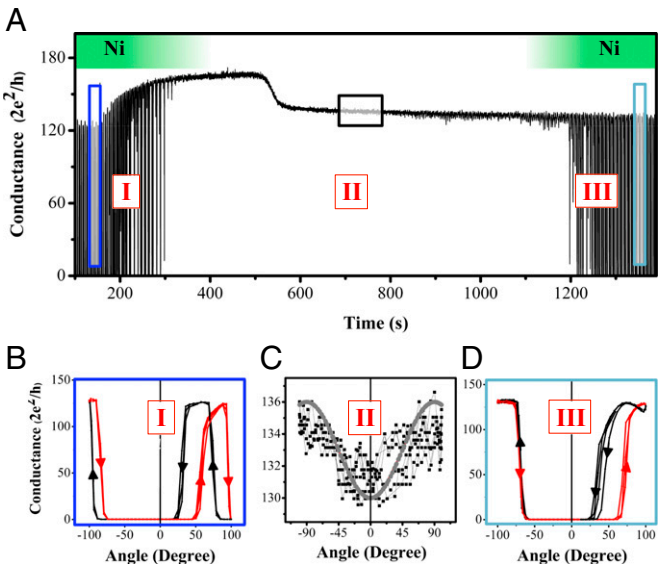

Fig. 2. Evolution of the anisotropic magnetoresistance of a Ni nanocontact when modifying the chemical environment. (*A*) Time evolution of the conductance under oscillating (0.5 Hz) rotation of the applied magnetic field of constant 0.8-T amplitude. The electroplating Ni solution is initially present (zone I), replaced with the buffer electrolyte solution (zone II), and reinstated (zone III), with the green bars indicating the presence of Ni^{++} ions. The rectangles correspond to the area used for reconstructing the AMR curves *B*, *C*, and *D*, corresponding to stages of experiments I, II, and III, respectively. A $\cos^2$ fit of *D*, expected for a metallic bulk Ni contact, is shown. Note the color-coding in *B* and *D* to differentiate the sweep directions.

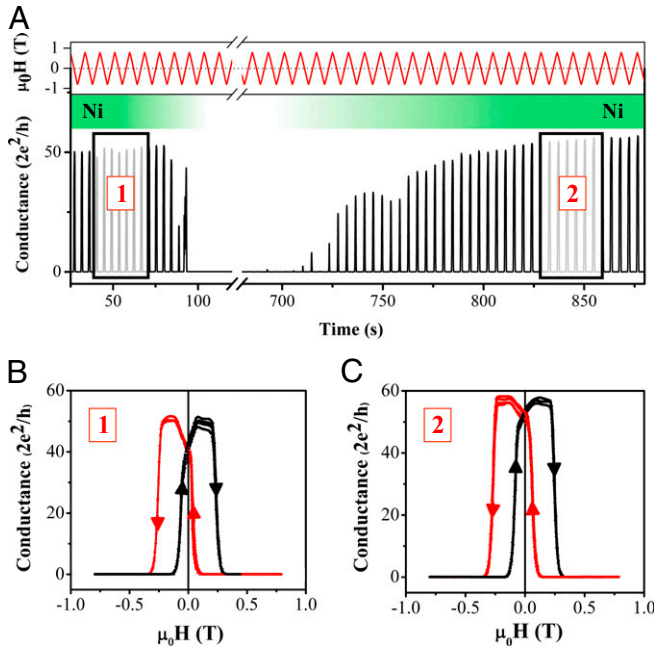

Fig. 3. Evolution of the magnetoresistance of a Ni nanocontact when modifying the chemical environment. (*A*) Time evolution of conductance during the whole experiment, with the oscillation of the varying applied field (at two slightly different rates) between ±0.8 T shown at top. When Ni ions are present (green area), during the initial 1 and final 2 conditions, a large oscillation of the sample conductance relates to the sweeping of the applied field. Eliminating the Ni ions from the solution results in an open contact; (*B* and *C*) related MR curves corresponding to time zones 1 and 2, indicating huge MR properties, recovered when reinstating the initial electrochemical environment.

continuous in amplitude (Fig. S1) when decreasing (increasing) the Ni ions concentrations. Our data clearly indicate that a model of conduction in a solid-state device is not appropriate here. They show unambiguously that Ni ions in the solution are at the origin of the remarkable AMR (MR).

A model detailing the influence of a magnetic field on paramagnetic ions can explain our findings. The paramagnetic Ni ions, of concentration C (in mol m^{-3}) in a solution, with molar magnetic susceptibility χ_m, (in m^3 mol^{-1}), are attracted to regions of high magnetic induction B (in tesla) with forces of density (in N m^{-3}):

$$\vec{f}_{\nabla} = \frac{C\chi_m}{2\mu_0}\vec{\nabla}\left(B^2\right)$$

where $\mu_0 = 4\pi\ 10^{-7}$ H m^{-1} (16). This "magnetic field gradient force" is proportional to the product of the scale-invariant field B with its gradient ∇B. The latter increases when decreasing the size of the system, and is therefore exacerbated at the nanoscale. This force prevails over forces related to the magnitude of B, and not its gradient. Magnetohydrodynamics usually refer to the Lorentz force, with the magnetic field modifying the trajectories of the electric current lines, and creating convection possibly modifying electrochemical equilibrium (17) or imposing chirality (18) when significant current densities are involved. In our case, with plating current densities not exceeding 5 μA/mm^2, the Lorentz force density remains below 100 N/m^3 (for our magnetic field in the 1-T range), shown below to be several orders of magnitude smaller than the gradient force near our nanostructures.

Quantitative insight of the predominant magnetic gradient force in our device geometry is obtained using a micromagnetic code, which accounts for the structure of the magnetization and the resulting magnetostatic field (19, 20) (see details in *SI Text*). We limit ourselves to the saturated state, expected for Ni when applied fields exceed 0.5 T, and corresponding to our AMR experimental conditions. This avoids ambiguity in the conclusions, as our modeling does not require any hypothesis for the magnetic configuration at low fields, where the relaxed state can be highly dependent on nanoscale minute defects in the real material geometry (Fig. 1*A*). We find that our planar electrodes design creates a gradient field exceeding 10^7 T/m. Such huge field gradients rival the highest values reported in the literature on single-spin detection using scanning probe techniques (7, 21), where the highest magnetic gradient is a prerequisite for measurement sensitivity. The force field directions and amplitudes in our calculations are illustrated in Fig. 3, using a dimensionless susceptibility $C\chi_m = 7.5\ 10^{-5}$ for a 1.8 M Ni^{++} paramagnetic ions concentration taking into account the diamagnetic property of water (see details in ref. 6). When the electrodes are magnetized along their length, or in a longitudinal direction with respect to the current direction, the force field of approximately radial symmetry reaches a magnitude of 10^9 Nm^{-3}. It exceeds by three orders of magnitude the largest value we found in the literature (22). The transverse magnetization case produces a local inversion of the force field, being now repulsive for ions residing at the edge of the nanogap, with magnitudes similar to the longitudinal case (Fig. 4, with more details in Fig. S2 and Table S1).

While magnetic forces are commonly used for positioning micro- or nano-size magnetic particles, they cannot stabilize molecules: A single paramagnetic molecule, with a spin S (not exceeding a small multiple of 1/2), cannot gain more than $1/2g^2\mu_B^2 S(S+1)B^2/3\ k_B T$ energy when attracted by a field B at temperature T. This is in the range of the Zeeman splitting energy, not exceeding the milli-Kelvin energy range in fields of the 1-T range. Magnetic fields can possibly modify chemical reactions rates and yields when they proceed via spin correlated radical pair intermediates. These spin chemistry effects (23) can occur in a wide range of applied fields, depending on the

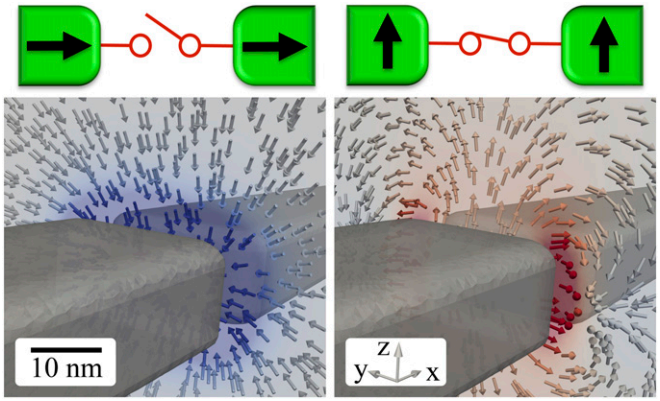

Fig. 4. Magnetic gradient force density field for nanoscale Ni electrodes. (*Upper*) Diagrams sketch the relaxed magnetization orientation in the electrodes, with a related broken or straight line symbolizing an open and closed electric contact. The electrodes are made of rectangular bars 300 nm long, 30 nm wide, and 16 nm high, with slightly rounded corners. (*Lower Left*) The external field of 0.8-T magnitude is applied along the longitudinal direction x. (*Lower Right*) The field is applied along the transversal direction y. The vector field reveals the direction of the forces. The color code indicates the amplitude of the forces, attractive (blue) in the longitudinal case and repulsive (red) in the transverse case. The maximum color intensity corresponds to a magnitude of 10^9 N/m^3. More quantitative details can be found in *SI Text*.

thermodynamic or quantum mechanical mechanism involved. The smallness of the Zeeman splitting magnetic energy can require rather large magnetic fields (of the order of 10 T) to impact the reaction (24). The hyperfine field, typically of the order of 0.1 T, can also significantly modify the lifetime of radical species, in the so-called "normal magnetic field effect," extensively studied for photosynthesis. Lower-field effects, down to submilli-Tesla field range, are of increasing importance, owing to the societal concerns about their effect on health (25). Note that these effects are unlikely to apply to our case, where the nanogaps always experience a significant field of 0.4–1 T for AMR studies, whatever the orientation of the external magnetic field is. Furthermore, correlated radical pairs typically result from a photoexcitation process, not applying in our case.

The thermal energy scale of 300 K also relates to Brownian motion, which controls diffusive forces, of the order of $RT\nabla C$ per unit volume in a gradient of concentration ∇C. There is general agreement in the literature (6, 22, 26, 27) that the diffusive forces dominate magnetic forces by orders of magnitude. Our scaling reasoning, explaining the numerical enhancement of the magnetic force field for our case, also applies to the diffusive forces. Magnetic gradient forces can nevertheless modify the convective flow around the electrodes in the presence of a transverse concentration gradient of electroactive species, possibly increasing the concentrations gradient and therefore enhancing diffusion (27, 28). Indeed, electrochemical studies showed that magnetic gradient (29) or Lorentz (30) (negligible in our case) forces near working electrodes can possibly change the residency time of paramagnetic species at the electrodes and shift the kinetics and equilibrium of the reactions (see, for example, refs. 22 and 28 and references therein).

In our case, with force fields larger by orders of magnitude, the magnetic gradient force must impact even more the chemical equilibria of the redox reactions (Fig. 4). The observed hysteresis in the AMR curves of Fig. 2 can be explained by the irreversibility of the redox chemical reactions involving the Ni^{++} ions. The observed open/closed switch of conductance under applied field can be mapped to the potentiostatic conditions V_{open}, V_{close}, where open, respectively closed, nanocontacts are favored. Experimentally, the difference between these two potential values is around 100 mV. The nonreversibility of the redox reactions makes this difference dependent on the sample's history, typically decreasing from initial values as large as 300 mV under successive open−close potential sequences. This provides a straightforward rough estimate of the contribution of the magnetic field to the free energy of the system, i.e., on the order of 10 kJ/mol (~100 meV/molecule), tunable through magnetic control of the electrodes. This value is large enough to overcome an energy activation barrier, modify significantly the reaction rates, or provide opportunities to (de)stabilize weak chemical bonds. For example, we recently found that a magnetic (sub)layer was necessary to self-assemble highly conductive supramolecular architectures between electrodes with nanoscale separation (31). As this particular self-assembly is controlled by the presence of paramagnetic radicals, their attraction to magnetic electrodes might drive the delicate chemical equilibrium toward self-construction. More generally, the stability of supramolecular architectures, where energetic contributions to the total free energy of the order of k_BT can significantly impact the molecular configurations, can therefore become sensitive to the magnetic forces at the vicinity of magnetic nanostructures. This opens interesting possibilities for acting on chemical processes relevant to life sciences, where supramolecular interactions prevail (32).

The field of magnetophoresis, currently implicitly related to magnetic manipulation of nanoparticles, is hereby extended to magnetic forces on paramagnetic molecules in solution, where extreme force field conditions in the vicinity of magnetic nanostructures can be generated without the need for a very large external magnetic field source. We have shown here that this phenomenon can be used for creating new types of spin-sensitive devices. We also propose a tabletop tool and methodology for influencing chemical reactions. Our findings suggest that the reaction yields or the chemical equilibrium, known to be sensitive to the magnetic field magnitude when intermediate radical species are involved, can also be influenced by the gradient of the magnetic field.

ACKNOWLEDGMENTS. We thank B. Lecomte, D. Spor, A. Boulard, and F. Chevrier for the experimental setup construction, M. Viret and S. Zanettini for discussions, and S. Haacke for support. We thank T. Ebbesen for suggestions on the manuscript and for his laboratory hospitality for focused ion beam processing. Partial financial support of the Agence Nationale de la Recherche (SUD 08-P056-036 and MULTISELF 11-BS08-06, Labex NIE 11-LABX-0058_NIE within the Investissement d'Avenir program ANR-10-IDEX-0002-02), the International Center for Frontier Research in Chemistry (icFRC, Strasbourg), and the technical support of the STnano cleanroom are also gratefully acknowledged.

1. Zutić I, Fabian J, Das Sarma S (2004) Spintronics: Fundamentals and applications. *Rev Mod Phys* 76(2):323–410.
2. Wolf SA, et al. (2001) Spintronics: A spin-based electronics vision for the future. *Science* 294(5546):1488–1495.
3. Johnson M (2004) *Magnetoelectronics* (Elsevier, Amsterdam).
4. Graham DL, Ferreira HA, Freitas PP (2004) Magnetoresistive-based biosensors and biochips. *Trends Biotechnol* 22(9):455–462.
5. Dobson J (2008) Remote control of cellular behaviour with magnetic nanoparticles. *Nat Nanotechnol* 3(3):139–143.
6. Coey JMD, Aogaki R, Byrne F, Stamenov P (2009) Magnetic stabilization and vorticity in submillimeter paramagnetic liquid tubes. *Proc Natl Acad Sci USA* 106(22):8811–8817.
7. Rugar D, Budakian R, Mamin HJ, Chui BW (2004) Single spin detection by magnetic resonance force microscopy. *Nature* 430(6997):329–332.
8. Yang CS, Zhang C, Redepenning J, Doudin B (2004) In situ magnetoresistance of Ni nanocontact. *Appl Phys Lett* 84(15):2865–2867.
9. Popa PL, et al. (2011) Heteronanojunctions with atomic size control using a lab-on-chip electrochemical approach with integrated microfluidics. *Nanotechnology* 22(21):215302 1-7.
10. Yang CS, Zhang C, Redepenning J, Doudin B (2004) Anisotropy magnetoresistance of quantum ballistic nickel nanocontacts. *J Magn Magn Mater* 286:186–190.
11. Sokolov A, Zhang C, Tsymbal EY, Redepenning J, Doudin B (2007) Quantized magnetoresistance in atomic-size contacts. *Nat Nanotechnol* 2(3):171–175.
12. Agrait N, Yeyati AL, van Ruitenbeek JM (2003) Quantum properties of atomic-sized conductors. *Phys Rep* 377(2-3):81–279.
13. McGuire TR, Potter RI (1975) Anisotropic magnetoresistance in ferromagnetic 3d alloys. *IEEE Trans Magn* 11(4):1018–1038.
14. Müller M, et al. (2011) Switching the conductance of Dy nanocontacts by magnetostriction. *Nano Lett* 11(2):574–578.
15. Doudin B, Viret M (2008) Ballistic magnetoresistance? *J Phys Condens Matter* 20(8):083201.
16. Rosensweig A (1997) *Ferrohydrodynamics* (Dover, New York).
17. Monzon LMA, Coey JMD (2014) Magnetic fields in electrochemistry: The Lorentz force. A mini-review. *Electrochem Commun* 42:38–41.
18. Mogi I, Morimoto R, Aogaki R, Watanabe K (2013) Surface chirality induced by rotational electrodeposition in magnetic fields. *Sci Rep* 3:2574.
19. Fredkin DR, Koehler TR (1990) Hybrid method for computing demagnetizing fields. *IEEE Trans Magn* 26(2):415–417.
20. Gliga S, Hertel R, Schneider CM (2008) Switching a magnetic antivortex core with ultrashort field pulses. *J Appl Phys* 103(7):07B115.
21. Mamin HJ, Rettner CT, Sherwood MH, Gao L, Rugar D (2012) High field-gradient dysprosium tips for magnetic resonance force microscopy. *Appl Phys Lett* 100(1):013102.
22. Chaure NB, Coey JMD (2009) Enhanced oxygen reduction at composite electrodes producing a large magnetic gradient. *J Electrochem Soc* 156(3):F39–F46.
23. Steiner UE, Ulrich T (1989) Magnetic field effects in chemical kinetics and related phenomena. *Chem Rev* 89(1):51–147.
24. Steiner UE, Gilch P (2003) High magnetic fields in chemistry. *Theory and Expertiments I*, High Magnetic Fields Science and Technology, ed. Herlach F (World Scientific, Teaneck, NJ), Vol 2.
25. Timmel CR, Henbest KB (2004) A study of spin chemistry in weak magnetic fields. *Philos Trans A Math Phys Eng Sci* 362(1825):2573–2589.
26. Dunne P, Mazza L, Coey JMD (2011) Magnetic structuring of electrodeposits. *Phys Rev Lett* 107(2):024501.

27. Dunne P, Coey JMD (2012) Patterning metallic electrodeposits with magnet arrays. *Phys Rev B* 85(22):224411.
28. Uhlemann M, et al. (2013) Structured electrodeposition in magnetic gradient fields. *Eur Phys J Spec Top* 220(1):287–302.
29. Dass A, Counsil JA, Gao X, Leventis N (2005) Magnetic field effects on the open circuit potential of ferromagnetic electrodes in corroding solutions. *J Phys Chem B* 109(21):11065–11073.
30. Rhen FMF, Coey JMD (2007) Magnetic field induced modulation of anodic area: Rest potential analysis of Zn and Fe. *J Phys Chem C* 111(8):3412–3416.
31. Faramarzi V, et al. (2012) Light-triggered self-construction of supramolecular organic nanowires as metallic interconnects. *Nat Chem* 4(6):485–490.
32. Lehn JM (1985) Supramolecular chemistry: Receptors, catalysts, and carriers. *Science* 227(4689):849–856.

Supporting Information

Lunca Popa et al. 10.1073/pnas.1322828111

SI Text

Materials and Methods

Electrodes of Au(30 nm)/Ti(5nm) are patterned by e-beam lithography or focused-ion-beam milling. We use a nickel sulphamate bath [$Ni(SO_3NH_2)_2 \bullet 4H_2O$ 1.8M, $NiCl_2 \bullet 6H_2O$ 0.08M, H_3BO_3 0.6M, pH = 3.8], known for its low residual stress and good film quality (1). The 1.8 M concentration relates to the maximum salt solubility. The impedance between two adjacent electrodes (or the two sides of the nanojunction) is measured by lock-in ac techniques (typically at 500 Hz), under excitation voltage V_{AC}, of 4 $mV_{p\text{-}p.}$, small enough to ensure common electrochemical conditions for both sides of the junction. We checked by impedance spectroscopy that the leakage bath impedance was larger than 100 kΩ, with typical 200-kΩ values, in the frequency range 1 Hz to 1 kHz. We verified our setup stability by reproducing the results of Xie et al. (2) showing a reversible switching of Ag junctions between two quantized conductance values produced by a slight modification of the potentiostatic conditions.

The gradient force density is derived from the magnetostatic field, calculated using a hybrid finite element method/boundary elements method algorithm that solves Poisson's equation for the magnetic potential with open boundary conditions (3). Since the code was originally developed to calculate magnetostatic fields inside interacting ferromagnets, the field outside the electrodes is obtained by introducing a nonmagnetic volume between the electrodes (4). We use an irregular mesh of tetrahedral discretization cells with an average edge length of about 1.3 nm. The mesh consists of 3.2 10^5 nodes and 1.8 10^6 cells, including the nonmagnetic region in which the stray field near the electrodes is calculated. The shape of the electrodes was rounded to avoid numerical divergence at the edges.

In Fig. S2, we illustrate the differences between the real case, in which an external field $H_p = 0.8$ T pins the saturated magnetic orientation of the electrodes, and a hypothetical case, in which we assume the magnetic orientation to be the same under zero external field. In the latter case, the forces field around the electrodes results from the stray field (or demagnetizing field) only. While the nonzero external field acts as a multiplying factor for the force in the longitudinal case, its effect is more drastic in the transverse case: the sign of $(d|\vec{B}|)/dz$ is approximately inverted, and the radial component of the force can be strongly repulsive when $H_p = 0.8$ T (when it significantly overcomes the demagnetizing field magnitude).

The parameters used in Table S1 and Fig. 2 are:

$\mu_0 M_s = 0.616$ T
$C = 1800$ mol/m^3
$\chi = 42\ 10^{-9}$ m^3/mol.

Note that the magnitude of the field gradient can exceed 10^8 T/m if a ferromagnetic material of larger saturation magnetization value is used (Fe, Dy). Such a value should be compared with the large field gradient needed for magnetic resonance force microscopy, with recently published highest values not exceeding 10^7 T/m (5).

1. Watanabe T (2004) *Nano Plating - Microstructure Formation Theory of Plated Films and a Database of Plated Films* (Elsevier, New York).
2. Xie FQ, Nittler L, Obermair Ch, Schimmel T (2004) Gate-controlled atomic quantum switch. *Phys Rev Lett* 93(12):128303.
3. Fredkin DR, Koehler TR (1990) Hybrid method for computing demagnetizing fields. *IEEE Trans Magn* 26(2):415–417.
4. Gliga S, Hertel R, Schneider CM (2008) Switching a magnetic antivortex core with ultrashort field pulses. *J Appl Phys* 103(7):07B115.
5. Mamin HJ, Rettner CT, Sherwood MH, Gao L, Rugar D (2012) High field-gradient dysprosium tips for magnetic resonance force microscopy. *Appl Phys Lett* 100(1): 013102.

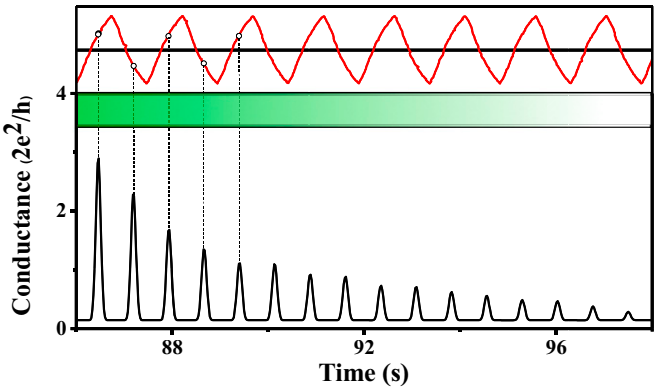

Fig. S1. Influence of the Ni ions concentration in the electrolyte on the MR properties of a Ni nanocontact. When exchanging the solutions, we suppose that the sample environment experiences a continuous variation of Ni ions concentration (fading green bar) within a few tens of seconds. The applied field is oscillating between ±0.8 T (red top line). The vertical dotted lines show the field values corresponding to the maxima of conductance, related to the coercive force of the electrodes magnetization (see MR curves of Fig. 3). These data show that the magnitude of the MR can be continuously varied with the Ni^{++} concentration and that smaller MR amplitudes occur when diminishing the Ni ions concentrations.

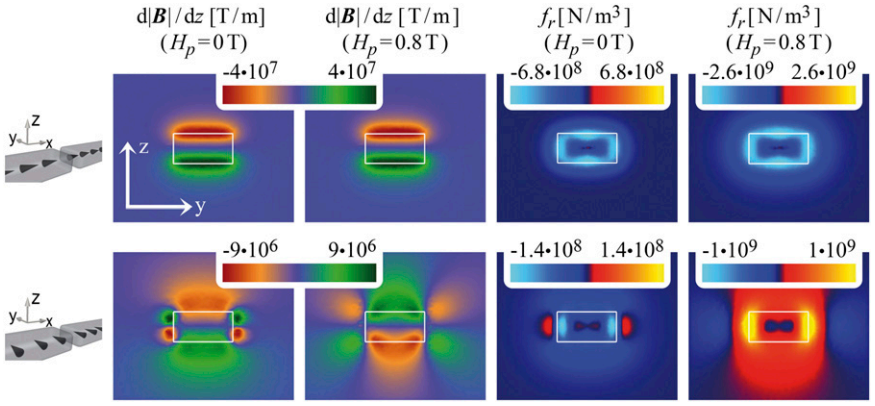

Fig. S2. Maps of the magnetic gradient and gradient force amplitudes. Color-coded 2D plot in the (*y*, *z*) plane of the magnitude of the gradient of the induction field along *z*, and the magnetic gradient force radial component. The two series of graphs correspond to the two magnetizations directions (longitudinal and transverse) indicated on the left and discussed in the main text, in their saturated relaxed magnetic state (arrows in the left drawings). The white square sketches the geometry of the electrodes projected on the plane, 30 nm × 16 nm in size.

Table S1. Minimum and maximum values of $(d|\vec{B}|)/dz$ and f_r for the two directions of electrode magnetization, corresponding to the cases of Fig. S2

	$\frac{d\|\vec{B}\|}{dz}$, T/m		f_r, N/m^3	
	H_p = 0 T	H_p = 0.8 T	H_p = 0 T	H_p = 0.8 T
x direction	Minimum: −4.2 10^7 T/m Maximum: 4.2 10^7 T/m	Minimum: −4.2 10^7 T/m Maximum: 4.2 10^7 T/m	Minimum: −6.8 10^8 N/m^3	Minimum: −2.6 10^9 N/m^3
y direction	Minimum: −0.92 10^7 T/m Maximum: 1.0 10^7 T/m	Minimum: −0.76 10^7 T/m Maximum: 7.7 10^7 T/m	Minimum: −14 10^7 N/m^3 Maximum: 2.0 10^7 N/m^3	Minimum: −9.5 10^7 T/m Maximum: 1.2 10^9 T/m